Hydrol. Earth Syst. Sci. Discuss., https://doi.org/10.5194/hess-2018-428
Manuscript under review for journal Hydrol. Earth Syst. Sci.
Discussion started: 15 August 2018

Hydrology and Earth System Sciences
Open Access
Discussions

Do climate-informed extreme value statistics improve the estimation of flood probabilities in Europe?

Eva Steirou[1], Lars Gerlitz[1], Heiko Apel[1], Xun Sun[2, 3], Bruno Merz[1, 4]

[1]Section Hydrology, GFZ German Research Center for Geosciences, Potsdam, 14473, Germany
[2]Key Laboratory of Geographic Information Science (Ministry of Education), East China Normal University, 200241, Shanghai, China
[3]Columbia Water Center, Earth Institute, Columbia University, New York, NY 10027, USA
[4]Institute of Earth and Environmental Science, University of Potsdam, Potsdam, 14476, Germany

Correspondence to: Eva Steirou (esteirou@gfz-potsdam.de), Xun Sun (xs2226@columbia.edu)

Abstract. The link between streamflow extremes and climatology has been widely studied during the last decades. However, a study investigating the effect of large-scale circulation variations on the distribution of seasonal discharge extremes at the European level is missing. Here we fit a climate-informed Generalized Extreme Value distribution (GEV) to about 600 streamflow records in Europe for each of the standard seasons, i.e. to winter, spring, summer and autumn maxima, and compare it with the classical GEV with parameters invariant in time. The study adopts a Bayesian framework and covers the period 1950 to 2016. Five indices with proven influence on the European climate are examined independently as covariates, namely the North Atlantic Oscillation (NAO), the East Atlantic pattern (EA), the East Atlantic / West Russian pattern (EA/WR), the Scandinavia pattern (SCA) and the Polar-Eurasian pattern (POL).

It is found that for a high percentage of stations the climate-informed model is preferred to the classical model, a result that provides evidence towards an improvement of the estimation of flood probabilities. Particularly for NAO during winter, a strong influence on streamflow extremes is detected for large parts of Europe (preferred to the classical GEV for 44% of the stations). Climate-informed fits are characterized by spatial coherence and form patterns that resemble relations between the climate indices and seasonal precipitation, suggesting a prominent role of the considered circulation modes for flood generation. For certain regions, such as Northwest Scandinavia and the British Isles, variations of the climate indices result in considerably different extreme value distributions and thus in highly different flood estimates for individual years. Plots of extreme streamflow with a probability of exceedance of 0.01 indicate that the deviation between the classical and climate-informed analysis concerns single years but can also persist for longer time periods.

1. Introduction

The understanding of extreme streamflow is a key issue for infrastructure design, flood risk management and (re-) insurance, and the estimation of flood probabilities has been in the focus of the scientific debate during recent decades. Traditionally, streamflow has been analysed with regard to associated hydro-climatic processes acting at the catchment scale. During recent years many studies have additionally focused on the link between local streamflow and larger-scale climate mechanisms, extending beyond the catchment boundaries (Merz et al., 2014). An early example can be found in Hirschboeck (1988), who provides a detailed explanation of relationships between floods and synoptic patterns in the USA. Large-scale atmospheric patterns acting at global or continental scales have been shown to significantly influence flood magnitude and frequency at the local and regional scale. Regional in this context refers to the joint consideration of several gauges. For example, Kiem et al. (2003)

stratified a regional flood index in Australia according to quantiles of the El Niño/Southern Oscillation (ENSO) index and showed that La Niña events are associated with a distinctly higher flood risk compared with El Niño events. Ward et al. (2014) found that peak discharges are strongly influenced by ENSO for a large fraction of catchments across the globe. Delgado et al. (2012) detected a dependence between the variance of the annual maximum flow at stations along the Mekong River and the intensity of the Western Pacific monsoon.

This perception of climate-influenced extremes has been incorporated in flood frequency analysis by including climatic variables as covariates of extreme value distribution parameters. It is therefore assumed that the probability density function (pdf) of streamflow is not constant in time but it is conditioned on external variables. This framework, usually called nonstationary, can be particularly useful for hydro-climatic studies since the influence of the climatic phenomena on the distribution of the hydrological target variable, such as extreme streamflow, can be considered (Sun et al., 2014). This means that the whole distribution as well as certain parts of the target variable distribution, such as the tails, can be assessed including the influence of the large scale climate phenomenon, and used for flood risk management, engineering design or reinsurance purposes. This conditional or nonstationary frequency analysis has been popularized in the field of hydrology and flood research during recent years. Different covariate types have been examined for their influence on flood extremes, e.g. time (e.g. Delgado et al., 2010; Sun et al., 2015), snow cover indices (Kwon et al., 2008), reservoir indices (López and Francés, 2013; Silva et al., 2017), population measures (Villarini et al., 2009) and large-scale atmospheric and oceanic fields and indices (Delgado et al., 2014; Renard and Lall, 2014). A review of nonstationary approaches for local frequency analyses is given by Khaliq et al. (2006), while some of their limitations are discussed by Koutsoyiannis and Montanari (2015) and Serinaldi and Kilsby (2015).

In this study, we focus on the European continent and the relation between streamflow extremes and the large-scale atmospheric circulation. The European climate is mainly influenced by pressure patterns acting at the broader region covering Europe, and the northern Atlantic. In particular five circulation modes have been shown to significantly modify the moisture fluxes into the European domain: the North Atlantic Oscillation (NAO), the East Atlantic (EA), the East Atlantic/Western Russia (EA/WR), the Scandinavia (SCA) and the Polar/Eurasia (POL) patterns (Bartolini et al., 2010; Casanueva et al., 2014; Rust et al., 2015; Steirou et al., 2017). These patterns represent the first five pressure modes north of 50°, derived by means of a rotated principle component analysis of monthly mean 500hPa geopotential height fields (Barnston and Livezey, 1987). The modes indicate the position and magnitude of large-scale atmospheric waves and thus control the strength and location of the northern hemispheric Jetstream. All modes are characterized by a particular pattern of large-scale winds and moisture fluxes and strongly affect near-surface climate conditions over vast parts of the northern hemisphere. Particularly NAO has been shown to significantly influence the European winter climate with positive (negative) anomalies of moisture fluxes, cyclone passages and precipitation over northern (southern) Europe during its positive state. A seasonal shift of the NAO pressure centres and moisture fluxes towards north during summer has been detected (Hurrell and Deser, 2009). EA, often referred to as a southward shifted NAO, is characterized by distinctly defined geopotential height anomalies and an associated influence on westerly moisture fluxes and local climate conditions over Great Britain (Comas-Bru and McDermott, 2014; Moore and Renfrew, 2012). EA/WR features two centres of action over Central Europe and Central Russia. During its positive state, a planetary ridge is located over north-western Europe, which reduces the advection of moist air masses (Krichak and Alpert, 2005). SCA is particularly active over northern Europe and triggers atmospheric blocking during its positive phase (Bueh and Nakamura, 2007). POL represents the strength of the pressure gradient between the polar regions and the mid-latitudes and thus controls the westerly circulation, particularly over northern Europe (Claud et al., 2007). Correlation maps, demonstrating links between these circulation modes and seasonal precipitation and temperature, are included in the Supplementary Material (Fig. S1-S4).

Apart from Northern Hemisphere modes, the El Niño-Southern Oscillation (ENSO) has been suggested to influence the European hydrology. Significant relations have been found with precipitation and different discharge indices (Guimarães Nobre et al., 2017; Mariotti et al., 2002; Steirou et al., 2017). However, in contrast to the above described circulation modes, ENSO does not shape the European climate and hydrology directly, but rather indirectly through the regulation of the phase of other large-scale modes, such as the EA (Iglesias et al., 2014). Other patterns acting at a smaller scale, such as the Mediterranean Oscillation (MO) and the Western Mediterranean Oscillation (WMO), have also been related with hydrological variables in Europe (Criado-Aldeanueva and Soto-Navarro, 2013; Dünkeloh and Jacobeit, 2003; Martin-Vide and Lopez-Bustins, 2006). However, such modes seem to have limited importance at the continental scale.

While the relation between European hydrology and large-scale circulation has attracted much attention and has been widely studied, only few studies have adopted a conditional flood frequency framework for the investigation of climate-flood interactions. Villarini et al. (2012) conducted a frequency analysis of annual maximum and peak-over-threshold discharge in Austria with NAO as a covariate. López and Francés (2013) examined maximum annual flows in Spain conditioned on the principal components of four winter climate modes: NAO, AO, MO and WMO. Still, a comprehensive study on streamflow extremes at the European scale has not yet been conducted.

Thus this study aims at a large-scale investigation of circulation-streamflow interactions for the entire European continent by adopting a flood frequency framework. We examine seasonal streamflow maxima from more than 600 gauges covering the entire European continent and particularly investigate the influence of the five major pressure modes that directly affect the European climate: NAO, EA, EA/WR, SCA and POL. In order to quantify the effect of important hydro-climatological processes for the streamflow regimes, we investigate contemporaneous relationships only, without considering any time lags. We identify regions with a consistent influence of each particular circulation index in order to explain the spatial coherence of flood frequency. The analysis is conducted at a seasonal scale in order to better account for the intra-annual variations of the circulation characteristics and the associated seasonal shift of climate-streamflow relationships. A Bayesian framework is adopted for the flood frequency analysis because of its advantages concerning the quantification of uncertainty.

2. Data and Methods

2.1 Streamflow data and circulation indices

The time period of our analysis is from 1950 to 2016, defined by the overlap between streamflow data and circulation indices. Daily streamflow data for the European continent were received from GRDC (Global Runoff Data Centre, 2017). From this dataset, gauges with record lengths of at least 50 years after 1950 and with a catchment area larger than 200 km^2 were selected. Small catchments are not considered, as they may be more prone to local phenomena, which could blur the large-scale atmospheric influence. In total, 649 stations covering North and Central Europe with the exception of Poland are considered. Due to the underrepresentation of Southern Europe, additional data from other sources satisfying the above mentioned criteria are included in the analysis. Five time series with monthly maximum discharges were obtained for Spain and one station with daily discharge was provided for Portugal. For details about these additional stations the reader is referred to Mediero et al. (2014,

Hydrol. Earth Syst. Sci. Discuss., https://doi.org/10.5194/hess-2018-428
Manuscript under review for journal Hydrol. Earth Syst. Sci.
Discussion started: 15 August 2018

Hydrology and Earth System Sciences
Open Access
Discussions

2015), respectively. Finally, one record with daily streamflow data was provided for Pontelagoscuro in Italy (Domeneghetti, 2017, personal communication). For each station, the maximum value of mean daily streamflow is derived for the four standard boreal seasons: winter (DJF), spring, (MAM), summer (JJA) and autumn (SON). Seasons with more than 20% missing values are not considered. Overall 586 records in winter, 604 in spring, 599 in summer and 597 for the autumn season are utilized for the analysis.

Time series of monthly circulation indices for the period 1950-2016 were retrieved from the Climate Prediction Center (CPC) of the National Oceanic and Atmospheric Administration (NOAA), (http://www.cpc.ncep.noaa.gov/data/teledoc/telecontents.shtml). We make use of the five indices mentioned in the introduction, namely, the NAO, EA, EA/WR, SCA and POL patterns. Seasonal mean climate indices are used for the adjustment of the extreme value distribution, however, we also examine whether the results differ if monthly values (in accordance with the observed flood date) are considered as covariate.

2.2 Flood frequency analysis – Competing models

The GEV with parameters invariant in time and with parameters conditioned on the climate indices are fitted to the seasonal maximum streamflow data. For the two types of models we use the terms "classical model" instead of stationary model and "climate-informed model" rather than "nonstationary model", respectively. It has been suggested that if covariates have a stochastic structure and no deterministic component, the resulting distribution is not truly nonstationary (Montanari and Koutsoyiannis, 2014; van Montfort and van Putten, 2002; Serinaldi and Kilsby, 2015). As our climate covariates have no distinguishable deterministic component (not shown), it is consequently not clear if they result in nonstationary models.

Each gauge is handled independently and site-specific parameters are derived. For the classical case the model is given as:

$$Y \sim GEV(\theta) \tag{1}$$

where Y is the vector of streamflow observations at a specific site and θ is the vector of length m of (time-invariant) distribution parameters. The classical GEV comprises m=3 parameters, namely a location parameter μ, a scale parameter σ and a shape parameter ξ.

In the Bayesian framework, the posterior pdf of the parameter vector is computed as follows, based on the Bayes theorem:

$$f(\theta|Y) \propto f(Y|\theta)f(\theta) \tag{2}$$

where f(θ) is the prior pdf of regression parameters and f(Y|θ) is the likelihood function:

$$f(Y|\theta) = \prod_t f(Y|\theta) \tag{3}$$

For the climate-informed distribution, parameters are assumed to be a function h_i of time-varying climate covariates $x(t)$. In the general case, Eq. (1) takes the form:

$$Y(t) \sim GEV(\theta(t)) \tag{4}$$

with

$$\theta_i(t) = h_i(x(t);\beta_i) \qquad i = \{1,2,\dots,m\} \tag{5}$$

Here β_i is the vector of (internal) parameters used in function h_i (not to be confused with parameters θ_i).

The climate-informed GEV is a generalization of the classical GEV. The likelihood function is then defined as:

$$f(Y|\theta) = \prod_t f(Y(t)|\theta(t)) = \prod_t f(Y(t)|h_1(x_t,\beta_1),h_2(x_t,\beta_2),\dots,h_m(x_t,\beta_m)) \tag{6}$$

The function h_i, linking the distribution parameters with climate covariates, is derived by means of a linear regression. Due to the brevity of observational records, we only examine conditional extreme value distributions with a time-varying location parameter. A preliminary analysis considering the effect of a covariate on both the location and scale parameter did not improve the results (not shown). The shape parameter is assumed to be constant as its estimation includes large uncertainties, even under the assumption of stationarity (Coles, 2001, Papalexiou and Koutsoyiannis, 2013; Silva et al., 2017). We derive conditional distributions of only one covariate at a time since we are interested in the separate effect of each individual climate index on flood quantiles.

Based on the above mentioned assumptions concerning model structure and the form of the function h_i, Eq. (5) can be simplified to:

$$\mu(t) = \mu_0 + \mu_1 x(t) \qquad (7)$$

Consequently, the conditional GEV comprises four parameters: scale and shape parameters, and intercept μ_0 and slope μ_1 for the location parameter. Since five different climate covariates *x(t)* are investigated, we construct six different models (one classical and five conditional) for each station and season. The posterior pdf of parameters in Eq. (2) for both the classical and conditional model is estimated using a No-U-Turn Sampler-Hamiltonian Monte Carlo approach (Hoffman and Gelman, 2014), implemented in Rstan, the R interface to Stan (Stan Development Team, 2017). Stan is a state-of-the-art platform for statistical modelling and high-performance statistical computation. For the fitting of the distribution we use non-informative priors, since no prior information is available. Five chains of 14,000 simulations, with the first half discarded as warmup period, are run for all parameters. Convergence is investigated by the potential scale reduction statistic, $\hat{R}$ (Gelman and Rubin, 1992). Following Gelman (1996), we assume convergence for values of $\hat{R}$ below 1.2. Thinning is applied to the post-warm up simulations to remove autocorrelation. Every tenth value from all chains is kept, leading to a final sample of 3,500 simulations.

2.3 Model selection

We apply a two-step methodology to select the optimal model among the classical and conditional competitors. First, we assess if the covariates have a significant effect on our extreme streamflow models by examining the posterior distribution of the slope μ_1 of the location parameters (Eq. 7). Conditional models are considered as significant if the zero value is not included in the 90% posterior interval of the slope parameter. A second criterion is additionally adopted in order to select the distribution with the best performance by taking into consideration that complex models with more parameters tend to fit the data better. The Deviance Information Criterion (DIC) (Spiegelhalter et al., 2002) is chosen for model selection. The DIC was preferred against two more common tools, the Akaike Information Criterion (AIC; Akaike, 1974) and the Bayesian Information Criterion (BIC; Schwarz, 1978), because it is based on the posterior distribution of the model parameters and thus includes parameter uncertainties, while the AIC and BIC are based on maximum likelihood estimates of parameters.

The deviance, used for the calculation of the DIC, is defined as:

$$\mathrm{D}(\theta) = -2\log(\mathrm{f}(\mathrm{y}|\theta)) \qquad (8)$$

where θ is the parameter vector. The DIC is then given by the following equation:

$$\mathrm{DIC} = \bar{D} + p_D \qquad (9)$$

where $\bar{D}$ is the expectation of the deviance with respect to the posterior distribution, and $p_D = \bar{D} + D(\bar{\theta})$ is the effective number of parameters (penalty for model complexity, following Spiegelhalter et al., 2002). Models with smaller DIC values are preferred.

Conditional models satisfying both criteria are preferred to the classical model. The model comparison is performed in two steps: first, for each station and season, each climate-informed competitor is pairwise compared to the classical GEV. Subsequently, the model with the overall best performance is identified.

2.4 Conditional flood quantiles

In the classical or stationary approach one can define the n-year return level as the high quantile of the examined variable for which the probability of exceedance is 1/n. In this case, the same probability of exceedance is assigned to same events in different years. The concept of return period can then be introduced as the reciprocal of the probability of exceedance of a specific value or return level of the examined variable (Cooley, 2013). In engineering practice, return period is often used to communicate risk and is understood either as the expected time interval at which the examined variable exceeds a certain threshold for the first time (average occurrence interval) or as the average of the time intervals between two exceedances of a given threshold (average recurrence interval) (Volpi et al., 2015). When the parameters of the distribution vary in time, as in the nonstationary or conditional frequency analysis, a different probability of exceedance is assigned to different years. In this case, the concept of return period becomes less straightforward to define. Thus, communicating risk by means of probabilities makes more sense (Cooley, 2013). Instead of the classical return levels the term "effective" return levels has been introduced (Gilleland and Katz, 2016) which represents the quantiles of the conditioned distribution under consideration of a particular value of the covariate during a given year.

Here we assess whether the consideration of climatic drivers leads to a significant alteration of flood "effective" return levels or conditional quantiles in individual years. Such an assessment allows to evaluate the applicability of the conditional extreme value analysis for engineering purposes. We quantify differences of flood quantiles during years with high and medium values of the considered circulation indices. Since the model is linear, the effect of high and low covariate values on the extreme value distribution quantiles is symmetrical and thus low covariate values are not considered. The 95^{th} and 50^{th} quantile of the considered climate index are chosen as high and medium index values, respectively. Index quantiles are calculated for the entire period 1950-2016.

Since a Bayesian framework is used, a certain covariate value does not correspond to a single flood quantile for a given probability of exceedance p. In our case, from the No-U-Turn sampling and after thinning, 3,500 post-warm up sets of parameters are obtained, each corresponding to a flood quantile (for given p). From all possible sets of parameters we choose the set corresponding to the maximum likelihood for the calculation of flood quantiles. Parameter uncertainty is not taken into consideration. It should be noticed that Monte Carlo Markov Chain (MCMC) methods, such as the No-U-Turn sampling, are not optimization methods and the maximum likelihood estimate from the sampling may slightly differ from the estimate from the standard maximum likelihood approach. A refinement of the modal estimate can be succeeded with the use of an optimization method to get closer to the posterior mode (Renard et al., 2013). In our case, because of the large size of posterior samples, the two methods were found to converge.

Based on this approach, the percent relative difference Y_p of the two flood quantiles for a particular probability of exceedance p, corresponding to the high and medium climate index quantiles, respectively, is calculated as follows:

$$Y_p = \frac{y_{p,h} - y_{p,m}}{y_{p,m}} (\%) \tag{10}$$

Hydrol. Earth Syst. Sci. Discuss., https://doi.org/10.5194/hess-2018-428
Manuscript under review for journal Hydrol. Earth Syst. Sci.
Discussion started: 15 August 2018

Hydrology and Earth System Sciences
Open Access
Discussions

where $y_{p,h}$ is a flood quantile for the probability p, incorporating a high value of the considered climate index (95[th] quantile). $y_{p,m}$ is the quantile value for the same probability p under consideration of the medium (50[th] quantile) climate index. The analysis is performed for probabilities of exceedance of 0.02 and 0.01.

2.5 Uncertainty analysis

In the previous chapters an automatic methodology for the choice of an adequate model and a discussion of flood quantiles for different covariate values is presented. However, a visual comparison of point estimates and uncertainty intervals of the classical and conditional models can be useful, since it illustrates the differences but also the plausibility and possible drawbacks of the competing models. For this reason, we plot the time series of flood quantiles for a probability of exceedance of 0.01 for selected gauges and covariates based on both the classical and the climate-informed extreme value distribution. Point estimates are derived for the set of parameters corresponding to the maximum likelihood (modal curve). Uncertainty of flood quantiles is quantified by means of posterior or credibility intervals, which are the Bayesian equivalent to frequentist confidence intervals, though differences considering the interpretation of the two types exist (Renard et al. 2013, Gelman et al., 2013).

3. Results

3.1 Spatial patterns of competing models

For all seasonal indices climate-informed models are preferred over the classical distribution for a large number of stations. Percentages are shown in Table 1 and spatial patterns are mapped in Fig. 1-2. The climate-informed fits form spatial clusters that resemble the correlations between the climate indices and average seasonal precipitation (Fig. S1-S4), while a relation with the correlations of seasonal mean temperature is not straightforward. Particularly for NAO a dipole pattern is evident in winter, with a positive influence on extreme discharge in northern and Central Europe and a negative relationship south of the Alps (Fig. 1). The intra-annual shift of the NAO pressure centres is well captured. The positive influence of NAO on flood magnitudes during summer is only detected for northern Scandinavia (Fig. 2). Similar dipole structures, resembling the correlations with seasonal mean precipitation, are found for other indices. However, there are some deviations from the precipitation patterns. For example contradicting results are found in Scandinavia during spring and summer for the SCA index. An opposite sign between correlations with precipitation and the slope of the location parameter can also be found during autumn in north-eastern Germany for the EA index.

NAO is the covariate with the highest number of significant fits in winter (44%) and autumn (32%) and EA in spring (33%) and summer (22%). High percentages of preferred climate-informed models are also found for EA and SCA in winter, which is the season where most indices are characterized by their strongest influence on the European climate (Table 1). Worst overall results are found for EA/WR in spring (4%) and POL in summer (7%). It can be argued that these two latter cases could occur solely by chance, however, results are coherent in space, which suggests a real influence of the circulation modes on the location parameter of the extreme value distributions, restricted though to certain sub-regions of Europe.

Similar spatial patterns are obtained from the same analysis if monthly covariates during the month of the seasonal discharge peaks are examined (Fig S5-S6). Clusters of stations with positive or negative slopes of the location parameter agree with those for seasonal indices, however in most cases the percentages of preferred fits are lower for the monthly covariates. In particular, the role of NAO in winter and autumn and of EA during the rest of the seasons is less pronounced. NAO and SCA are the covariates with the highest number of preferred fits in spring and EA during the rest of the seasons, together with EA/WR in summer (Table 2). Regarding the spatial patterns of preferred fits, deviations from those for seasonal covariates can be found for EA/WR, SCA and POL during spring and summer.

For all indices examined, a percentage of stations between 6 and 13%, depending on the season and the covariate, are characterized by lower DIC for the climate-informed model although the slope of the location parameter is not statistically significant (illustrated as yellow points in Fig. 1 and 2). No station records are characterized by higher DIC value for the climate-informed model without showing a significant slope. These results indicate that DIC is a weaker criterion for model selection than the slope significance at 10% level.

In order to illustrate the spatial structure of best models, the preferred model (classical or climate-informed) is mapped in Fig. 3 and 4 for each station for seasonal covariates. Spatial patterns do not resemble the pattern of significant fits for separate indices (Fig. 1, 2), since the influence of the selected climate modes on flood frequencies is overlapping for some regions and some of the indices are correlated for particular seasons. Winter (summer) is the season with the highest (lowest) overall percentage of preferred climate-informed models: 77% and 45%, respectively.

In winter, NAO is the most influential climate mode, being preferred over the other modes for 27% of the gauges. The largest influence of NAO on flood frequencies is detected in Central Europe, Great Britain and parts of Scandinavia (Fig. 3). The same regions show a high fraction of SCA-influenced models, which points towards a joint effect of NAO and SCA during winter. The two indices are significantly correlated during this season. EA is identified as the best covariate in winter for Great Britain. In spring an expansion of the EA influence towards Central Europe is detected. The NAO influence is shifted to the south during the transition seasons (spring and autumn) and is completely dissolved in summer. Patterns for SCA are heterogeneous throughout the year. The same results but for monthly covariates are shown in Fig. S7 and S8. Spatial patterns resemble those for seasonal covariates. Percentages of preferred climate-informed models are included in Tables 1 and 2.

3.2 Conditional quantiles and uncertainty analysis

In the previous section it is shown, that, models with monthly covariates do not outperform those with seasonal covariates. Hence, quantiles of climate indices are calculated at the seasonal scale only (Table 3). Figures 5 and 6 show the relative differences of seasonal flood quantiles for a probability of exceedance of 0.01 between a (hypothetical) year with a climate index value equal to the 95th index quantile and a year with an index value equal to the median. The patterns for probabilities of exceedance of 0.02 are very similar (not shown).

For a probability of exceedance of 0.01, relative differences higher than 20% and up to 28% are detected in winter for NAO, EA and SCA. For the rest of the seasons maximum relative differences are lower than 20% with highest values for EA/WR in autumn (marginally below 20%). In spring and summer the highest value is considerably lower, about 13% for NAO, EA, SCA and POL in spring and EA in summer.

A difference of 5-10% is quite common for NAO in winter. For example a station record with a positive slope of the location parameter and a probability of exceedance of 0.01 for a maximum seasonal discharge value of 600 m^3/s during years characterized by a medium NAO index, has an effective return level between 630 and 660 m^3/s during years with a highly positive NAO state. Particularly for Great Britain and Scandinavia high relative differences for different indices are found in winter. Differences of extreme discharge higher than 10% are characteristic for variations of the EA index in south-eastern Britain and for EA/WR in Norway. Some stations with high differences are also found in Norway and northern Britain for NAO and SCA in spring. Summer is characterized by low relative differences, below 5% for most stations. On the contrary, in autumn clusters of stations with medium to high differences (higher than 5% and locally exceeding 10%) are found in Scandinavia for NAO and EA/WR, in entire northern Europe for EA and in the Alpine region and southern Great Britain for SCA.

The results for three selected gauges with high relative differences $Y_{0.01}$ are presented in detail. The selected stations cover different characteristic combinations with regard to the investigated season and the considered covariate. The time series of discharge values with a probability of exceedance of 0.01 are illustrated based on the conditional distribution considering the three indices with the lowest DIC (Fig. 7). Details about the streamflow gauges and the climate-informed fits are given in Table 4 and Table 5, respectively.

Results show, that the conditional and unconditional uncertainty bounds can differ considerably, particularly for models with a high relative difference $Y_{0.01}$ and a low DIC (subplots A1, B1 and C1 in Fig. 7). Obviously conditional uncertainty bounds vary with time. Remarkably, modal values of conditional and unconditional models also diverge. For example, for the station Asbro 3 in Sweden, strongly different results are obtained by the classical and the NAO-conditional model in winter, particularly for the period 1960-1970, which was dominated by negative NAO conditions and reduced winter precipitation amounts over Northern Europe. The same applies for the station Teston in Great Britain during the period 1960-1980, if EA is considered as a covariate. These results show that the climate-informed models can modulate the estimated flood risk for single years or longer periods and thus substantially deviate from the estimation based on the classical distributions.

For models characterized by small relative differences or insignificant slopes of the location parameter (subplots A3, B3 and C3), conditional uncertainty bounds tend to converge to a straight line resembling the classical case. The classical case is theoretically a subcase of the climate-informed model. However, the two models are fitted independently and the two intervals do not always overlap. The uncertainty bounds of the climate-informed fits can be narrower or wider than those of the classical model. They are also remarkably asymmetrical, in contrary to uncertainty bounds that result from a method using a normal approximation. Asymmetrical intervals are associated with the shape parameter of the GEV and are not uncommon (see for example Zeng et al., 2017).

4. Discussion and conclusions

This study explored if a climate-informed flood frequency analysis improves the estimation of flood probabilities at the European scale. A site-specific model using a Bayesian framework was developed, and five Euro-Atlantic circulation modes were investigated as potential covariates: the North Atlantic Oscillation (NAO), the East Atlantic pattern (EA), the Scandinavia pattern (SCA) and the Polar/Eurasian pattern (POL). Streamflow was analysed at a seasonal time scale in order to account for the variable influence of the circulation modes on the European climate during different seasons of the year. Covariates were averaged and examined at both seasonal and monthly scales, contemporaneous to the season or month of the seasonal streamflow maxima, respectively.

The developed climate-informed models were compared to the classical GEV with time-invariant parameters. For most seasons and covariates investigated, the climate-informed models were preferred over the classical GEV for a high number of stations, with best results found in winter for NAO and EA, in spring for EA and in autumn for NAO (Table 1). Results were shown to be coherent in space, indicating that certain regions are influenced by particular circulation modes (Fig. 1-4). In winter 77% of the stations were found to be influenced by one of the climate modes which indicates a high potential for an improvement of flood probability estimations by including climate information into extreme value statistics. On the contrary, less than half of the stations examined were significantly affected by at least one of the five large-scale indices during summer season, indicating a rather convective and non-predictable precipitation regime (Table 1).

Based on the variability of the circulation indices, we identified regions that are characterized by preferred climate-informed fits and by steep slopes of the location parameter. The results indicate, that the inclusion of climate information into the extreme value analysis leads to highly varying flood quantile estimations for different probabilities of exceedance. Particularly for Northwest Scandinavia and the British Isles variations of the climate indices result in considerably different extreme value distributions and thus highly different flood estimates for individual years (Fig. 5-6). Plots of extreme streamflow under consideration of a probability of exceedance of 0.01 indicate that the deviation between the classical and climate-informed analysis concerns not only single years but can also persist for longer time periods (Fig. 7), which reflects the decadal-scale variability of NAO and other large-scale circulation indices.

Although the circulation indices examined are characterized by a high intra-seasonal variability, the seasonally averaged indices provided better fits compared with monthly values (Tables 1-2). This should be emphasized, since extreme precipitation events are most likely stronger related with monthly circulation states, which better represent the moisture fluxes into the target domain. On the contrary, the catchment wetness before the flood event is likely to be influenced by the seasonal mean circulation and the associated precipitation sums. Hence, our result suggests that the skill of climate informed extreme values distributions is to a significant part a consequence of the important link between catchment wetness and flooding. Thus we assume, in line with recent studies (Blöschl et al., 2017; Merz et al., 2018), that in many regions of Europe, catchment wetness plays an important role for flood generation.

For the selection of the best model among the classical and climate-informed two criteria were adopted: the DIC and the significance of the slope of the location parameter μ_1. For all indices and seasons, the DIC favoured the climate-informed models over the classical distribution for a larger number of stations compared to the slope significance. DIC has received some criticism for not adequately penalising complex models and tending to choose overfitted models (Silva et al., 2017; Spiegelhalter et al., 2014). Our results show that at least compared to the slope significance, DIC is a weaker criterion for model selection. A criterion comprising a higher penalty term for model complexity could alternatively be adopted. A more conservative version of DIC has been proposed by Ando (2011) but is not commonly used until today (Silva et al., 2017).

The described methodology can be complemented in several ways.

(a) Number of covariates

Single covariate models were developed, focusing on the separate effect of each individual climate mode. The methodology can be extended to a model considering several covariates at the same time. In that case, dependencies between the covariates, if existent, should be taken into consideration. López and Francés (2013) overcame this problem by using the principal components of climatic indices as covariates for the flood frequency analysis.

(b) Symmetric and asymmetric influence

A symmetrical influence of the positive and negative phases of the climate indices on the extreme value distribution has been assumed in this study. However, an asymmetrical relation may better describe the effect of certain climate modes on streamflow extremes. For example, Sun et al. (2014) used an asymmetric piecewise-linear regression to account for the different effects of El Niño and La Niña on rainfall extremes in Southeast Queensland, Australia.

(c) Contemporaneous and lagged relationships

In this paper we considered contemporaneous relationships between streamflow extremes and pressure modes that directly shape the European climate and hydrology. However, lagged relationships may also prove more useful for flood risk management and the (re-)insurance industry, since they would allow forecasts of temporal variable flood quantiles for the following month or season. Therefore, we plan to operate the presented model in a forecast mode under consideration of different time lags between selected covariates and observed streamflow maxima. Our results suggest that catchment wetness has an important role in shaping seasonal maximum streamflow. Thus in a follow up study, we will systematically test the skill of various predictor variables, describing both the climate and catchment state, in forecasting runoff extremes in Europe.

Acknowledgements

The GRDC discharge dataset was obtained from The Global Runoff Data Centre, 56068 Koblenz, Germany. Alessio Domeneghetti is thanked for providing unpublished discharge data from Italy and Luis Mediero for providing discharge data from Spain and Portugal. Dr. Xun Sun is supported by the National Key R&D Program of China (No. 2017YFE0100700) and Shanghai Pujiang Program (No. 17PJ1402500). This study was conducted in the frame of the projects “Conditional flood frequency analysis: exploring the link of flood frequency to catchment state and climate variations” and “The link of flood frequency to catchment state and climate variations”, two joined research initiatives between AXA Global P&C and GFZ, Potsdam. The authors wish to acknowledge AXA Research Fund for the financial support.

References

Akaike, H.: New look at statistical-model identification, IEEE Trans. Automat. Control, AC 19 (6), 716–723, 1974.

Barnston, A. G. and Livezey, R. E.: Classification, seasonality and persistence of low-frequency atmospheric circulation patterns, Mon. Weather Rev., 115, 1083–1126, 1987.

Bartolini, E., Claps, P. and D’Odorico, P.: Connecting European snow cover variability with large scale atmospheric patterns, Adv. Geosci., 26, 93–97, doi:10.5194/adgeo-26-93-2010, 2010.

Blöschl, G., Hall, J., Parajka, J., Perdigão, R. A. P., Merz, B., Arheimer, B., Aronica, G. T., Bilibashi, A., Bonacci, O., Borga, M., Čanjevac, I., Castellarin, A., Chirico, G. B., Claps, P., Fiala, K., Frolova, N., Gorbachova, L., Gül, A., Hannaford, J., Harrigan, S., Kireeva, M., Kiss, A., Kjeldsen, T. R., Kohnová, S., Koskela, J. J., Ledvinka, O., Macdonald, N., Mavrova-Guirguinova, M., Mediero, L., Merz, R., Molnar, P., Montanari, A., Murphy, C., Osuch, M., Ovcharuk, V., Radevski, I., Rogger, M., Salinas, J. L., Sauquet, E., Šraj, M., Szolgay, J., Viglione, A., Volpi, E., Wilson, D., Zaimi, K. and Živković, N.: Changing climate shifts timing of European floods, Science (80-.)., 357(6351), 588–590, doi:10.1126/science.aan2506, 2017.

Bueh, C. and Nakamura, H.: Scandinavian pattern and its climatic impact, Q. J. R. Meteorol. Soc., 133(629), 2117–2131, doi:10.1002/qj.173, 2007.

Casanueva, A., Rodríguez-Puebla, C., Frías, M. D. and González-Reviriego, N.: Variability of extreme precipitation over Europe and its relationships with teleconnection patterns, Hydrol. Earth Syst. Sci., 18(2), 709–725, doi:10.5194/hess-18-709-2014, 2014.

Claud, C., Duchiron, B. and Terray, P.: Associations between large-scale atmospheric circulation and polar low developments over the North Atlantic during winter, J. Geophys. Res. Atmos., 112(12), 1–16, doi:10.1029/2006JD008251, 2007.

Comas-Bru, L. and McDermott, F.: Impacts of the EA and SCA patterns on the European twentieth century NAO-winter climate relationship, Q. J. R. Meteorol. Soc., 140(679), 354–363, doi:10.1002/qj.2158, 2014.

Cooley, D.: Return periods and return levels under climate change, in Extremes in a Changing Climate, pp. 97–114, Springer, Amster- dam, Netherlands, 2013.

Criado-Aldeanueva, F. and Soto-Navarro, F. J.: The Mediterranean Oscillation Teleconnection Index: Station-Based versus Principal Component Paradigms, Adv. Meteorol., 2013, 1–10, doi:10.1155/2013/738501, 2013.

Delgado, J. M., Apel, H. and Merz, B.: Flood trends and variability in the Mekong river, Hydrol. Earth Syst. Sci., 14(3), 407–418, doi:10.5194/hess-14-407-2010, 2010.

Delgado, J. M., Merz, B. and Apel, H.: A climate-flood link for the lower Mekong River, Hydrol. Earth Syst. Sci., 16(5), 1533–1541, doi:10.5194/hess-16-1533-2012, 2012.

Delgado, J. M., Merz, B. and Apel, H.: Projecting flood hazard under climate change: An alternative approach to model chains, Nat. Hazards Earth Syst. Sci., 14(6), 1579–1589, doi:10.5194/nhess-14-1579-2014, 2014.

Dünkeloh, A. and Jacobeit, J.: Circulation dynamics of Mediterranean precipitation variability 1948-98, Int. J. Climatol., 23(15), 1843–1866, doi:10.1002/joc.973, 2003.

Gelman, A. and Rubin, D. B.: Inference from Iterative Simulation Using Multiple Sequences, Stat. Sci., 7(4), 457–472, doi:10.1214/ss/1177011136, 1992.

Gelman A.: Inference and monitoring convergence. In: Gilks W. R., Richardson S, Spiegelhalter D. J. (eds) Markov chain Monte Carlo in practice. Chapman & Hall, New York, pp 131–143, 1996.

Gelman A., Carlin J. B., Stern H. S., Dunson D. B., Vehtari A., Rubin D. B.: Bayesian Data Analysis. 3rd edition. Chapman & Hall/CRC, London, 2013.

Gilleland, E. and Katz, R. W.: extRemes 2.0: An Extreme Value Analysis Package in R, J. Stat. Softw., 72(8), doi:10.18637/jss.v072.i08, 2016.

Guimarães Nobre, G., Jongman, B., Aerts, J. and Ward, P. J.: The role of climate variability in extreme floods in Europe, Environ. Res. Lett., 12(8), 084012, doi:10.1088/1748-9326/aa7c22, 2017.

Hirschboeck, K. K.: Flood hydroclimatology. In V. R. Baker (Ed.), Flood geomorphology (pp. 27-49). Wiley-Interscience, 1988.

Hoffman M. D., Gelman A.: The No-U-Turn sampler: adaptively setting path lengths in Hamiltonian Monte Carlo. J. Mach. Learn. Res. 15: 1593–1623, 2014.

Hurrell, J. W. and Deser, C.: North Atlantic climate variability: The role of the North Atlantic Oscillation, J. Mar. Syst., 78(1), 28–41, doi:10.1016/j.jmarsys.2008.11.026, 2009.

Iglesias, I., Lorenzo, M. N. and Taboada, J. J.: Seasonal Predictability of the East Atlantic Pattern from Sea Surface Temperatures, edited by J. M. Dias, PLoS One, 9(1), e86439, doi:10.1371/journal.pone.0086439, 2014.

Khaliq, M. N., Ouarda, T. B. M. J., Ondo, J. C., Gachon, P. and Bobée, B.: Frequency analysis of a sequence of dependent and/or non-stationary hydro-meteorological observations: A review, J. Hydrol., 329(3–4), 534–552, doi:10.1016/j.jhydrol.2006.03.004, 2006.

Kiem, A. S., Franks, S. W. and Kuczera, G.: Multi-decadal variability of flood risk, Geophys. Res. Lett., 30(2), 1035, doi:10.1029/2002GL015992, 2003.

Koutsoyiannis, D. and Montanari, A.: Negligent killing of scientific concepts: the stationarity case, Hydrol. Sci. J., 60(7–8), 1174–1183, doi:10.1080/02626667.2014.959959, 2015.

Krichak, S. O. and Alpert, P.: Decadal trends in the east Atlantic-west Russia pattern and Mediterranean precipitation, Int. J. Climatol., 25(2), 183–192, doi:10.1002/joc.1124, 2005.

Kwon, H.-H., Brown, C. and Lall, U.: Climate informed flood frequency analysis and prediction in Montana using hierarchical Bayesian modeling, Geophys. Res. Lett., 35(5), L05404, doi:10.1029/2007GL032220, 2008.

López, J. and Francés, F.: Non-stationary flood frequency analysis in continental Spanish rivers, using climate and reservoir indices as external covariates, Hydrol. Earth Syst. Sci., 17(8), 3189–3203, doi:10.5194/hess-17-3189-2013, 2013.

Mariotti, A., Zeng, N. and Lau, K.-M.: Euro-Mediterranean rainfall and ENSO—a seasonally varying relationship, Geophys. Res. Lett., 29(12), 1621, doi:10.1029/2001GL014248, 2002.

Martin-Vide, J. and Lopez-Bustins, J.-A.: The Western Mediterranean Oscillation and rainfall in the Iberian Peninsula, Int. J. Climatol., 26(11), 1455–1475, doi:10.1002/joc.1388, 2006.

Mediero, L., Santilla´n, D., Garrote, L. and Granados, A.: Detection and attribution of trends in magnitude, frequency and timing of floods in Spain, J. Hydrol., 517, 1072–1088, doi:10.1016/j.jhydrol.2014.06.040, 2014.

Mediero, L., Kjeldsen, T. R., Macdonald, N., Kohnova, S., Merz, B., Vorogushyn, S., Wilson, D., Alburquerque, T., Blöschl, G., Bogdanowicz, E., Castellarin, A., Hall, J., Kobold, M., Kriauciuniene, J., Lang, M., Madsen, H., Onuşluel Gül, G., Perdigão, R. A. P., Roald, L. A., Salinas, J. L., Toumazis, A. D., Veijalainen, N. and Þórarinsson, Ó.: Identification of coherent flood regions across Europe by using the longest streamflow records, J. Hydrol., 528, 341–360, doi:10.1016/j.jhydrol.2015.06.016, 2015.

Merz, B., Aerts, J., Arnbjerg-Nielsen, K., Baldi, M., Becker, A., Bichet, A., Blöschl, G., Bouwer, L. M., Brauer, A., Cioffi, F., Delgado, J. M., Gocht, M., Guzzetti, F., Harrigan, S., Hirschboeck, K., Kilsby, C., Kron, W., Kwon, H.-H., Lall, U., Merz, R., Nissen, K., Salvatti, P., Swierczynski, T., Ulbrich, U., Viglione, A., Ward, P. J., Weiler, M., Wilhelm, B. and Nied, M.: Floods and climate: emerging perspectives for flood risk assessment and management, Nat. Hazards Earth Syst. Sci., 14(7), 1921–1942, doi:10.5194/nhess-14-1921-2014, 2014.

Merz, B., Dung, N. V., Apel, H., Gerlitz, L., Schröter, K., Steirou, E. and Vorogushyn, S.: Spatial coherence of flood-rich and flood-poor periods across Germany, J. Hydrol., 559, 813–826, doi:10.1016/j.jhydrol.2018.02.082, 2018.

Montanari, A. and Koutsoyiannis, D.: Modeling and mitigating natural hazards: Stationary is immortal, Water Resour. Res., 9748–9756, doi:10.1002/2014WR016092.Received, 2014.

van Montfort, M. A. J. and van Putten, B.: A comment on modelling extremes : Links between Multi-Component Extreme Value and General Extreme Value distributions, J. Hydrol. (New Zealand), 41(2), 197–202, 2002.

Moore, G. W. K. and Renfrew, I. A.: Cold European winters: interplay between the NAO and the East Atlantic mode, Atmos. Sci. Lett., 13(1), 1–8, doi:10.1002/asl.356, 2012.

Papalexiou, S. M. and Koutsoyiannis, D.: Battle of extreme value distributions: A global survey on extreme daily rainfall, Water Resour. Res., 49(1), 187–201, doi:10.1029/2012WR012557, 2013.

Renard, B. and Lall, U.: Regional frequency analysis conditioned on large-scale atmospheric or oceanic fields, Water Resour. Res., 50(12), 9536–9554, doi:10.1002/2014WR016277, 2014.

Renard, B., Sun, X., Lang, M.: Bayesian methods for non-stationary extreme value analysis. In: AghaKouchak, A., Easterling, D., Hsu, K., Schubert, S., Sorooshian, S. (Eds.), Extremes in a Changing Climate: Detection, Analysis and Uncertainty. Water Science and Technology Library, Springer, Netherlands, pp. 39–95, 2013.

Rust, H. W., Richling, A., Bissolli, P. and Ulbrich, U.: Linking teleconnection patterns to European temperature – a multiple linear regression model, Meteorol. Zeitschrift, 24(4), 411–423, doi:10.1127/metz/2015/0642, 2015.

Schwarz, G.: Estimating the dimension of a model. Ann. Stat. 6 (2), 461–464, 1978.

Serinaldi, F. and Kilsby, C. G.: Stationarity is undead: Uncertainty dominates the distribution of extremes, Adv. Water Resour., 77, 17–36, doi:10.1016/j.advwatres.2014.12.013, 2015.

Silva, A. T., Portela, M. M., Naghettini, M. and Fernandes, W.: A Bayesian peaks-over-threshold analysis of floods in the Itajaí-açu River under stationarity and nonstationarity, Stoch. Environ. Res. Risk Assess., 31(1), 185–204, doi:10.1007/s00477-015-1184-4, 2017.

Spiegelhalter, D. J., Best, N. G., Carlin, B. P. and van der Linde, A.: Bayesian Measures of Model Complexity and Fit, J. R. Stat. Soc. Ser. B (Statistical Methodol., 64(4), 583–639, doi:10.1111/1467-9868.00353, 2002.

Spiegelhalter, D. J., Best, N. G., Carlin, B. P. and Linde, A. Van Der: The deviance information criterion: 12 years on (with discussion), J. R. Stat. Soc. Ser. B, 64, 485–493, 2014.

Stan Development Team: RStan: the R interface to Stan. R package version 2.16.2. http://mc-stan.org, 2017.

Steirou, E., Gerlitz, L., Apel, H. and Merz, B.: Links between large-scale circulation patterns and streamflow in Central Europe: A review, J. Hydrol., 549, doi:10.1016/j.jhydrol.2017.04.003, 2017.

Sun, X., Thyer, M., Renard, B. and Lang, M.: A general regional frequency analysis framework for quantifying local-scale climate effects: A case study of ENSO effects on Southeast Queensland rainfall, J. Hydrol., 512, 53–68, doi:10.1016/j.jhydrol.2014.02.025, 2014.

Sun, X., Lall, U., Merz, B. and Dung, N. V.: Hierarchical Bayesian clustering for nonstationary flood frequency analysis: Application to trends of annual maximum flow in Germany, Water Resour. Res., 51(8), 6586–6601, doi:10.1002/2015WR017117, 2015.

Villarini, G., Smith, J. A., Serinaldi, F., Bales, J., Bates, P. D. and Krajewski, W. F.: Flood frequency analysis for nonstationary annual peak records in an urban drainage basin, Adv. Water Resour., 32(8), 1255–1266, doi:10.1016/j.advwatres.2009.05.003, 2009.

Villarini, G., Smith, J. A., Serinaldi, F., Ntelekos, A. A. and Schwarz, U.: Analyses of extreme flooding in Austria over the period 1951-2006, Int. J. Climatol., 32(8), 1178–1192, doi:10.1002/joc.2331, 2012.

Volpi, E., Fiori, A., Grimaldi, S., Lombardo, F. and Koutsoyiannis, D.: One hundred years of return period: Strengths and limitations, Water Resour. Res., 51(10), 8570–8585, doi:10.1002/2015WR017820, 2015.

Ward, P. J., Eisner, S., Flörke, M., Dettinger, M. D. and Kummu, M.: Annual flood sensitivities to El Niño–Southern Oscillation at the global scale, Hydrol. Earth Syst. Sci., 18(1), 47–66, doi:10.5194/hess-18-47-2014, 2014.

Zeng, H., Sun, X., Lall, U. and Feng, P.: Nonstationary extreme flood/rainfall frequency analysis informed by large-scale oceanic fields for Xidayang Reservoir in North China, Int. J. Climatol., 37(10), 3810–3820, doi:10.1002/joc.4955, 2017.

Figures

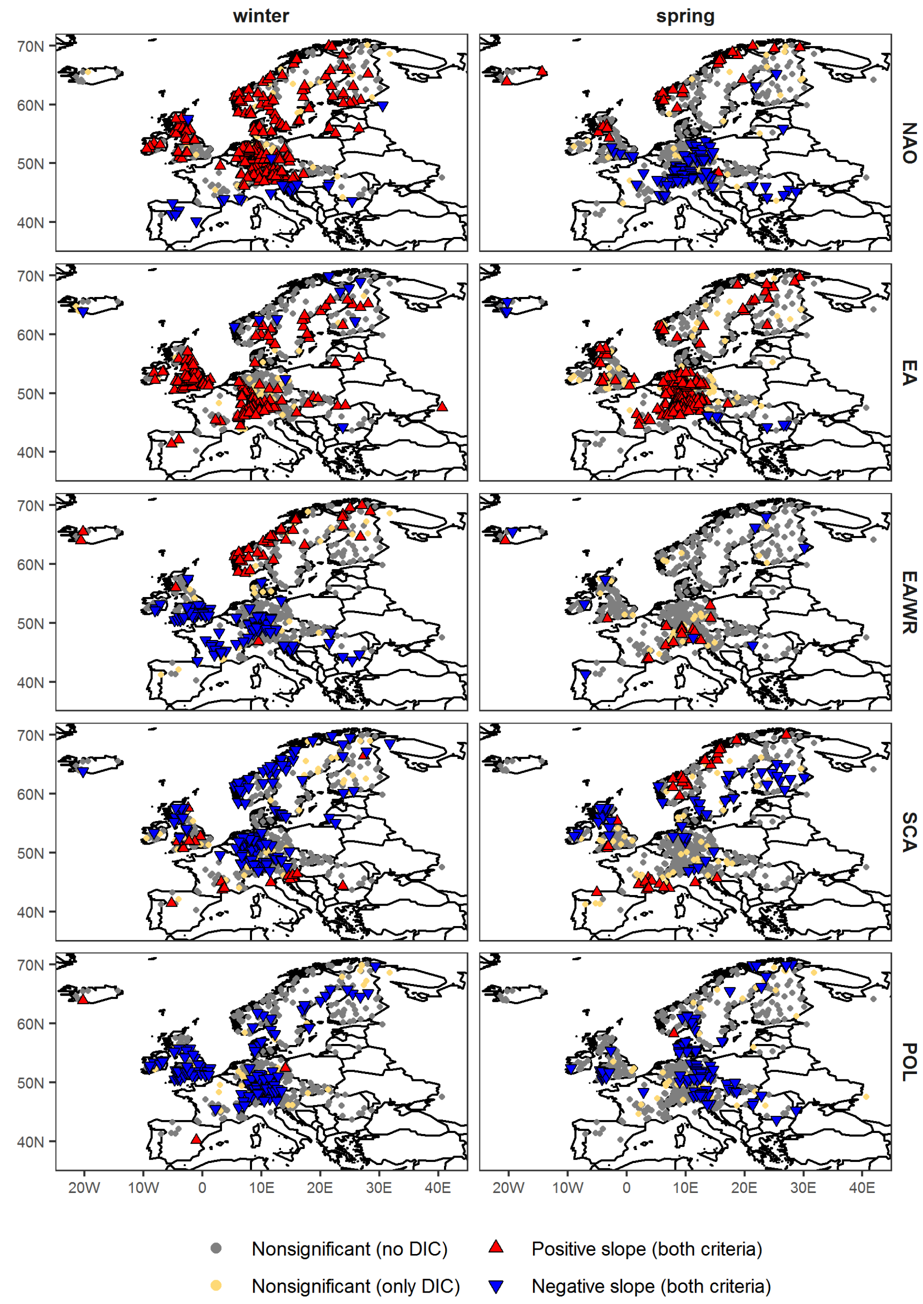

550 **Figure 1: Results comparing the climate-informed and the classical GEV models for all covariates examined for the winter and spring season. Nonsignificant models preferred only by the DIC (yellow points) are plotted on top of stations for which climate-informed models were not chosen by any of the two criteria (grey points). Preferred climate-informed models chosen by both criteria (blue/red triangles) are illustrated on top of the other models so that they can be better distinguished.**

Hydrol. Earth Syst. Sci. Discuss., https://doi.org/10.5194/hess-2018-428
Manuscript under review for journal Hydrol. Earth Syst. Sci.
Discussion started: 15 August 2018

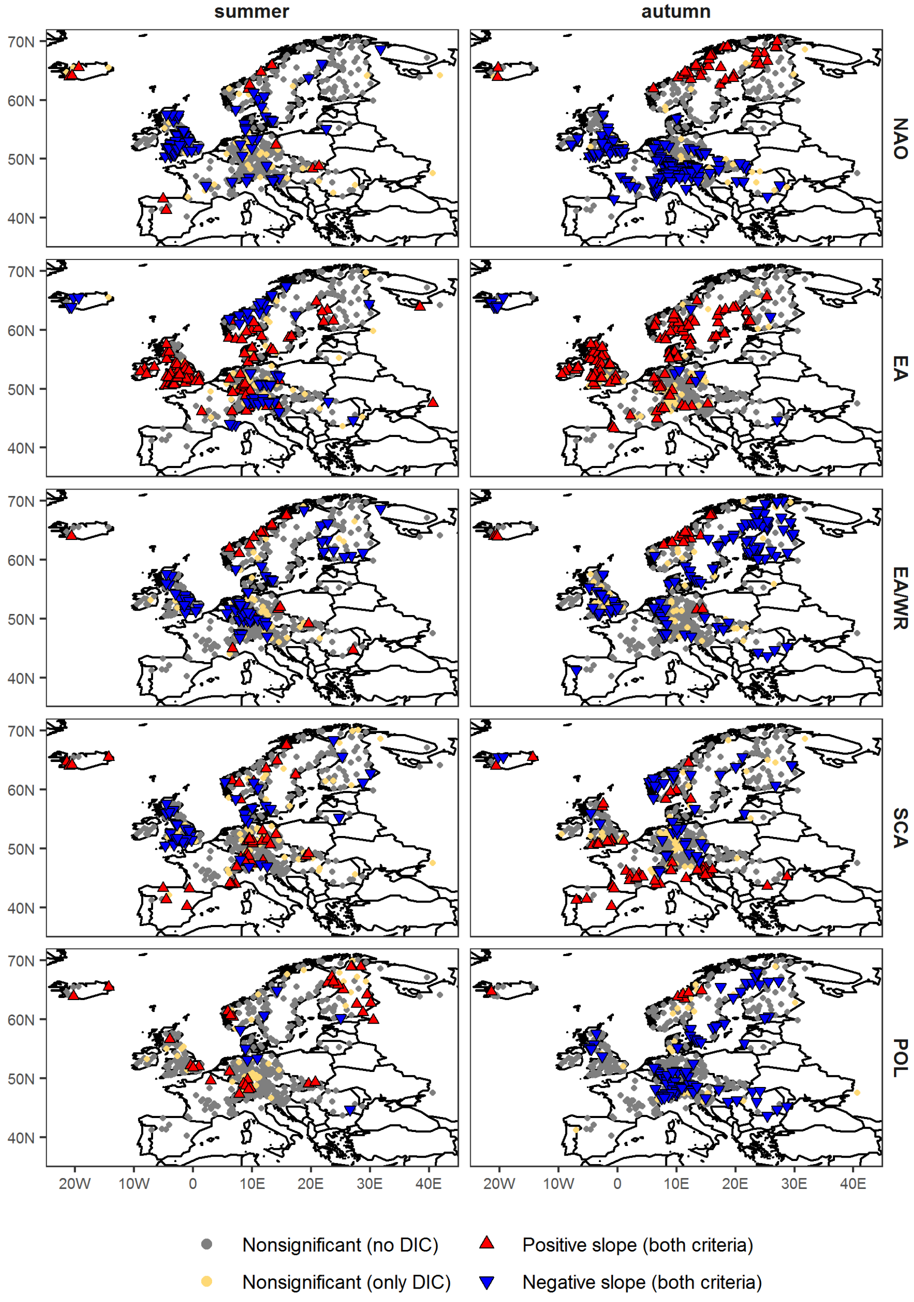

555 **Figure 2: Same as Fig. 1 but for the summer and autumn season.**

Hydrol. Earth Syst. Sci. Discuss., https://doi.org/10.5194/hess-2018-428
Manuscript under review for journal Hydrol. Earth Syst. Sci.
Discussion started: 15 August 2018

Hydrology and Earth System Sciences
Discussions

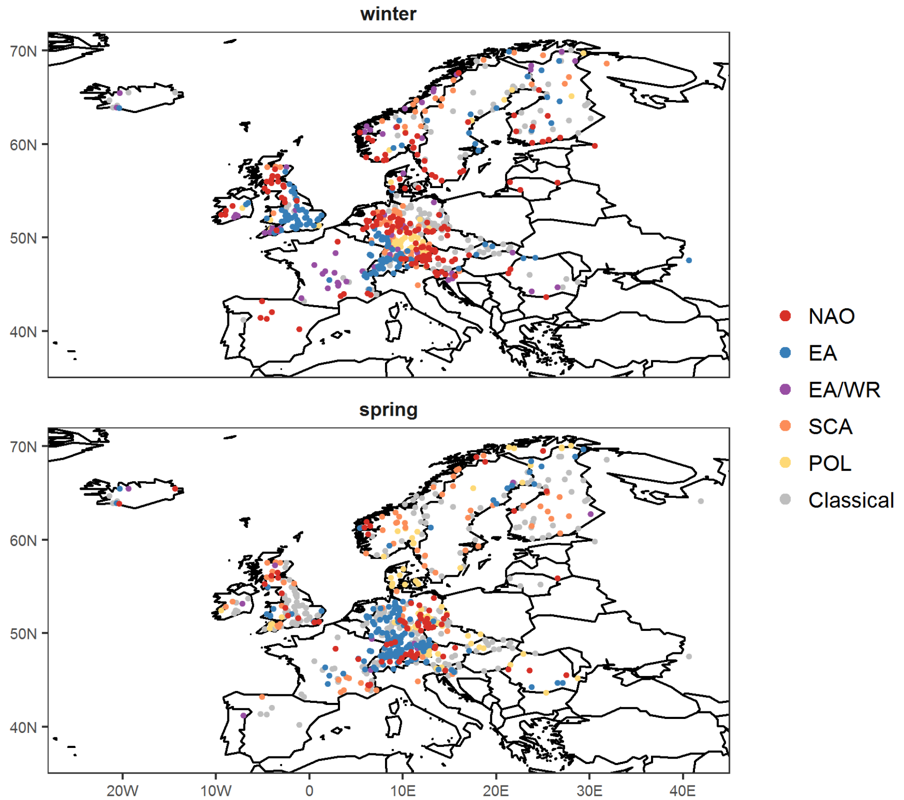

560 **Figure 3: Best overall models among the five climate-informed and classical GEV tested for the winter and spring season. Mean seasonal covariates are examined.**

Hydrol. Earth Syst. Sci. Discuss., https://doi.org/10.5194/hess-2018-428
Manuscript under review for journal Hydrol. Earth Syst. Sci.
Discussion started: 15 August 2018

Hydrology and Earth System Sciences
Discussions
Open Access

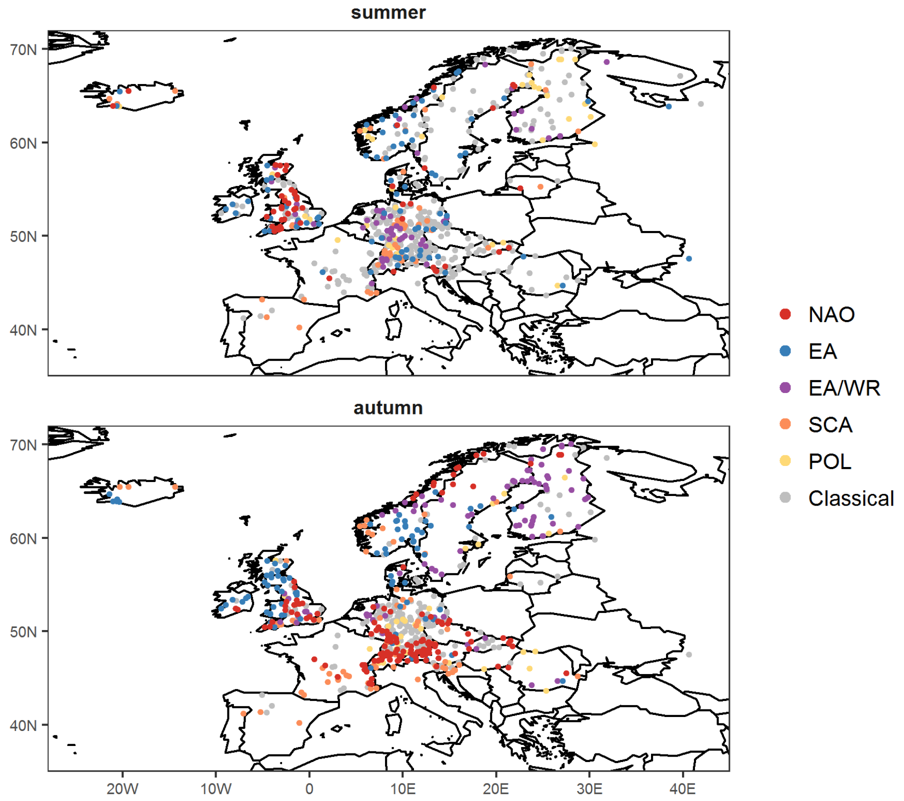

Figure 4: Same as Fig. 3 but for the summer and autumn season.

Hydrology and Earth System Sciences
Open Access
Discussions

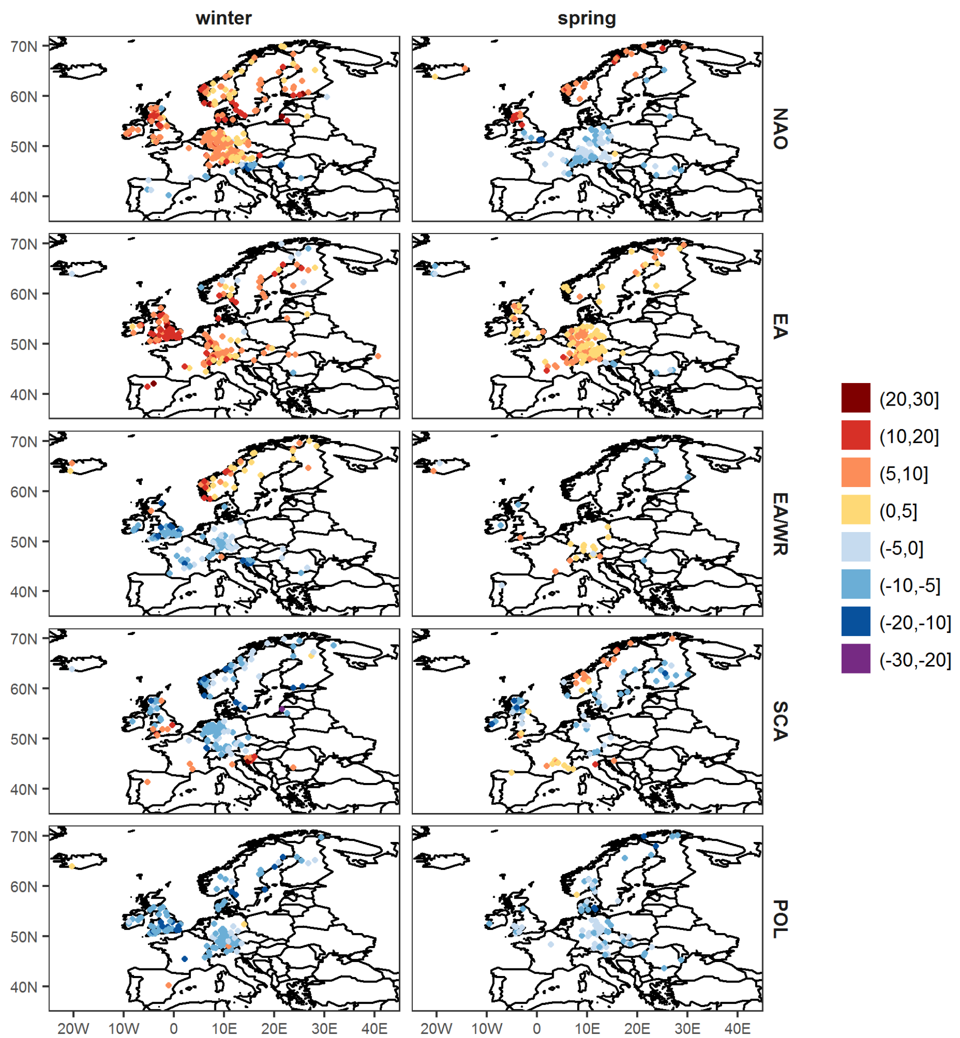

565 **Figure 5: Percent relative difference of the streamflow for an exceedance probability of 0.01 between a (hypothetical) year with a climate index value equal to the 95th quantile and a year with an index value equal to the median index. Results are shown for winter and spring and seasonal mean covariates.**

Hydrol. Earth Syst. Sci. Discuss., https://doi.org/10.5194/hess-2018-428
Manuscript under review for journal Hydrol. Earth Syst. Sci.
Discussion started: 15 August 2018

Hydrology and Earth System Sciences
Open Access
Discussions

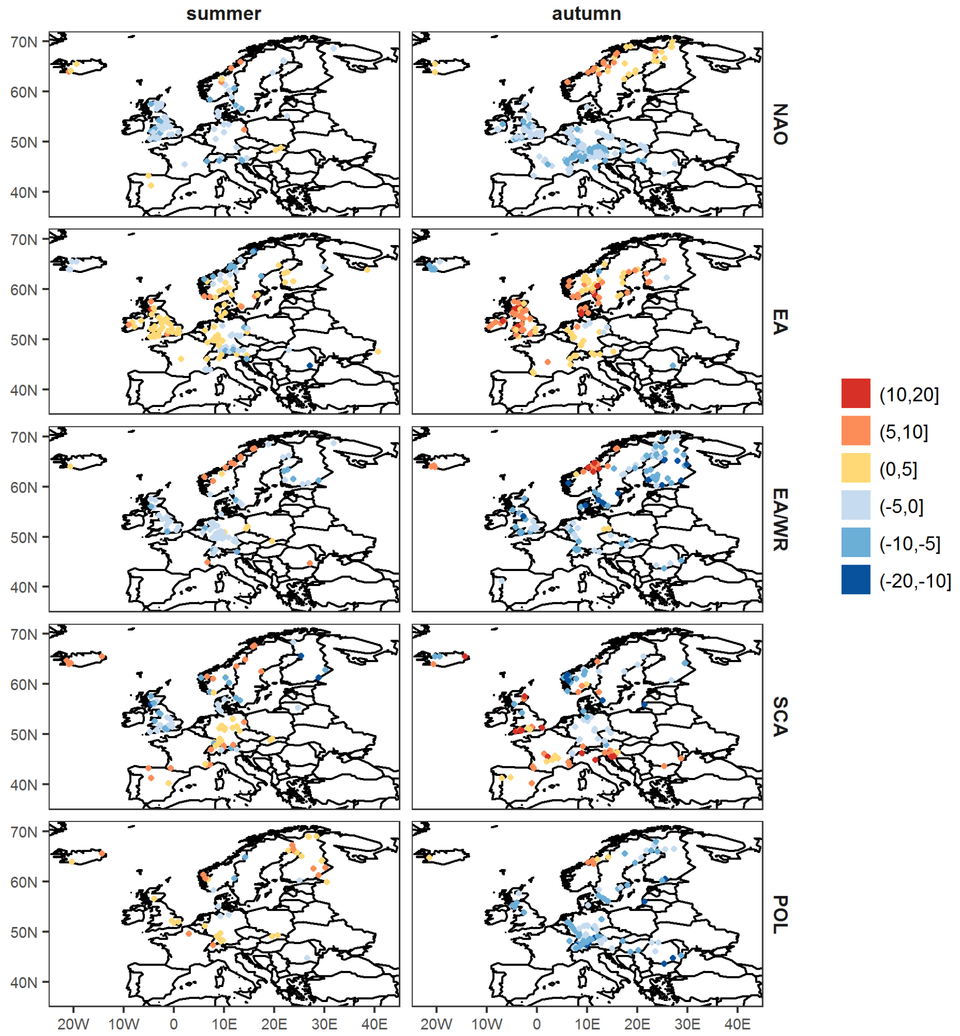

570 **Figure 6: Same as Fig. 5 but for the summer and autumn season.**

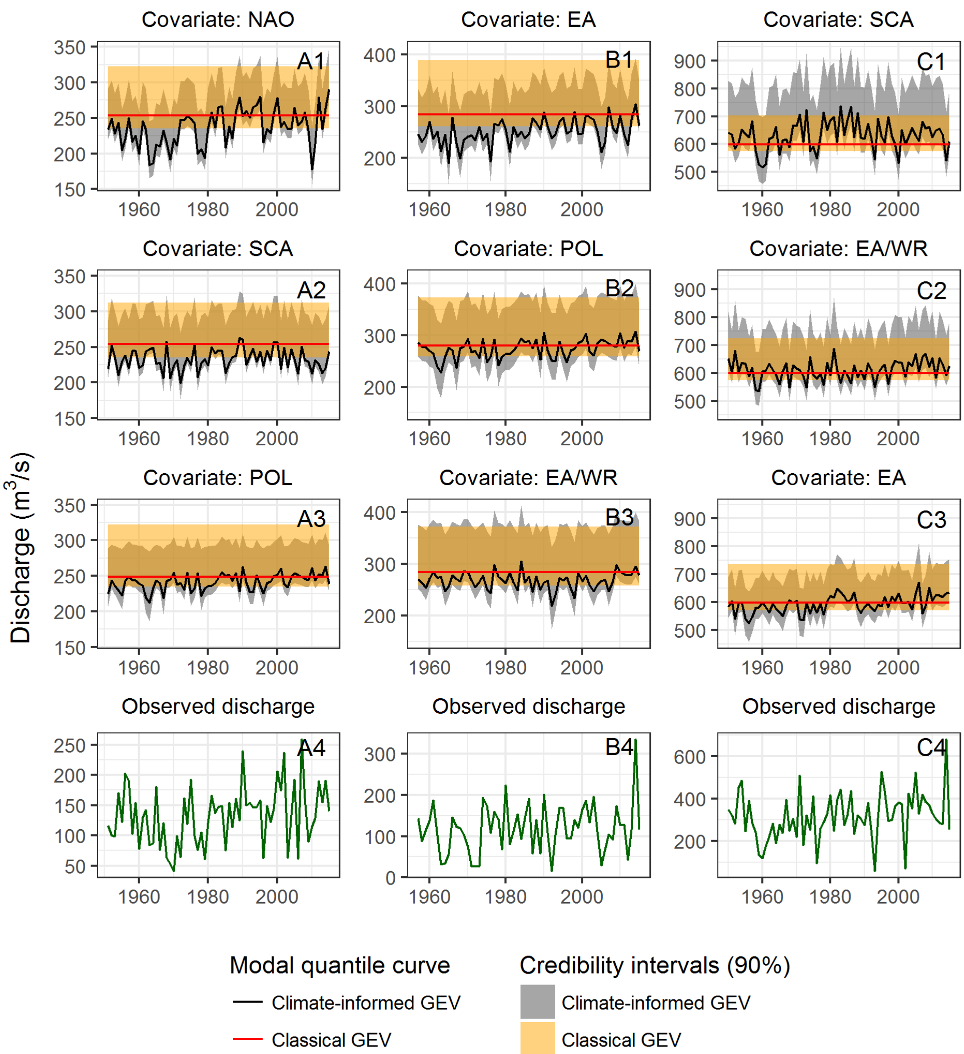

575 **Figure 7: Annual maximum discharge time series (lower panel: 4) and climate-informed quantiles (upper panels: 1-3) with credibility intervals for P(Y>y=0.01) for three selected gauges (Table 4, 5). Climate-informed quantiles are compared with those of the classical GEV. The three best climate-informed models based on the DIC are shown for each site, with increasing DIC from top to bottom.**

580

Tables

Table 1: Percentage of stations with climate-informed fits preferred to the classical GEV model. Indicated is the result of the pairwise comparison of each covariate with the classical model and the percentage of preferred fits for each covariate when all models are compared (in brackets). Results are shown per season and for mean seasonal covariates.

Index	Winter	Spring	Summer	Autumn
NAO	44 (27)	21 (12)	14 (9)	32 (24)
EA	30 (21)	30 (25)	22 (13)	20 (14)
EA/WR	23 (11)	4 (2)	14 (9)	21 (14)
SCA	25 (11)	13 (11)	15 (8)	16 (12)
POL	23 (8)	14 (10)	7 (6)	15 (5)
All indices	(77)	(61)	(45)	(68)

Table 2: Same as Table 1 but for monthly covariates at the same month as the seasonal streamflow extremes.

Index	Winter	Spring	Summer	Autumn
NAO	21 (16)	17 (12)	15 (11)	16 (10)
EA	22 (17)	15 (12)	16 (11)	22 (18)
EA/WR	9 (6)	14 (10)	16 (13)	20 (13)
SCA	16 (10)	17 (12)	13 (10)	14 (9)
POL	13 (9)	16 (12)	8 (6)	11 (7)
All indices	(42)	(59)	(50)	(56)

Table 3: Seasonal quantiles of the five climate indices: median and in the parenthesis the 95th quantile are provided.

Index	Winter	Spring	Summer	Autumn
NAO	-0.26 (1.04)	-0.15 (0.84)	0.02 (1.14)	0.17 (0.96)
EA	-0.37 (1.07)	-0.13 (0.70)	-0.07 (0.80)	-0.19 (0.69)
EA/WR	-0.19 (0.78)	-0.04 (0.78)	0.15 (1.23)	0.11 (1.29)
SCA	0.21 (1.25)	0.05 (0.90)	0.09 (1.33)	0.21 (1.44)
POL	0.11 (1.44)	0.07 (0.90)	-0.11 (0.94)	-0.02 (0.91)

Table 4: General information about selected sites shown in Fig. 7. Ref. code is the number of the subplot of Fig. 7.

Ref. code	Station name	Country	GRDC No	Latitude	Longitude	Catchment size (km^2)
A	ASBRO 3	Sweden	6233100	57.240	12.310	2160.2
B	TESTON	United Kingdom	6607851	51.251	0.447	1256.1
C	BULKEN	Norway	6731200	60.630	6.280	1102.0

Table 5: Climate-informed results as shown in Fig. 7. Ref. code is the number of the subplot of Fig. 7. Mean seasonal covariates for the same season as streamflow extremes are examined. dDIC is the difference from the DIC value of the classical distribution. $Y_{0.01}$ is the percent relative difference of streamflow with P(Y>y=0.01) for the 95th quantile of the covariate ($y_{0.01,h}$) and of streamflow with P(Y>y=0.01) for the median ($y_{0.01,m}$). The sign of the slope is reported if it is significantly different than zero at the 10% significance level.

Ref. code	Season	Covariate	dDIC	Slope	$Y_{0.01}$ [%]	$y_{0.01,m}$ [m^3/s]	$y_{0.01,h}$ [m^3/s]
A	Winter	NAO	-22.6	Positive	19.7	239.5	281.3
		SCA	-5.0	Negative	-9.2	236.2	211.9
		POL	-0.5	Nonsignificant	-	-	-
B	Winter	EA	-9.6	Positive	16.1	247.9	291.7
		POL	-5.8	Negative	-13.5	263.5	229.3
		EA/WR	-4.0	Negative	-7.8	269.2	246.6
C	Autumn	SCA	-14.3	Negative	-15.4	643.2	547.0
		EA/WR	-5.3	Negative	-10.9	602.8	539.5
		EA	-3.5	Positive	7.1	593.9	636.8